Molecular Crystals and Liquid Crystals
Publication details, including instructions for authors and subscription information:
http://www.tandfonline.com/loi/gmcl16

Studies on Disc-like Molecules

Michio Sorai [a], Kazuhiro Tsuji [a], Hiroshi Suga [a] & Syŭzŏ Seki [a]

[a] Department of Chemistry, Faculty of Science, Osaka University, Toyonaka, Osaka, 560, Japan

Version of record first published: 20 Apr 2011.

To cite this article: Michio Sorai , Kazuhiro Tsuji , Hiroshi Suga & Syŭzŏ Seki (1980): Studies on Disc-like Molecules, Molecular Crystals and Liquid Crystals, 59:1-2, 33-58

To link to this article: http://dx.doi.org/10.1080/00268948008073497

Mol. Cryst. Liq. Cryst., 1980, Vol. 80, pp. 33–58
0026-8941/80/5901–0033$04.50/0

Printed in the U.S.A.

Studies on Disc-like Molecules

I. Heat Capacity of Benzene-hexa-*n*-hexanoate from 13 to 393 K

MICHIO SORAI, KAZUHIRO TSUJI,† HIROSHI SUGA and SYÛZÔ SEKI†

Department of Chemistry, Faculty of Science, Osaka University, Toyonaka, Osaka 560, Japan.

(*Received July 23, 1979; in final form September 13, 1979*)

The heat capacity of benzene-hexa-*n*-hexanoate, $C_6(OCOC_5H_{11})_6$, with a purity of 99.98 mole per cent has been measured between 13 and 393 K. Four phase transitions were found at 251.58 (Phase IV → III), 291.46 (III → II), 348.27 (II → I) and 368.74 K (Phase I → liquid). The enthalpy and entropy of these transitions were determined to be 25.66 kJ mol^{-1}/102.67 J K^{-1} mol^{-1}; 12.27/46.11; 16.26/46.68; and 33.50/90.86, respectively. These phase transitions are regarded as a kind of successive phase transitions: the conformational melting progresses from the periphery of a molecule into its inside each time a phase transition takes place. The infrared and far infrared spectra remarkably depend on temperature; the noticeable changes observed with increasing temperature are a smearing effect of the intramolecular vibrational modes and a reduction of the number of infrared active bands. The spectra of Phase I are substantially the same as those of the liquid, indicating rapid motions of the paraffinic chains in Phase I. The phase transitions can be seen very clearly under a polarizing microscope. The optical texture of Phase I seems to be of crystal rather than of liquid crystal. The highest temperature "solid" phase (Phase I) was concluded here to be a highly disordered crystalline phase concerning conformations of the paraffinic chains.

1 INTRODUCTION

There exist a number of molecular crystals which consist of molecules having special geometries and are not directly transformed into a true isotropic liquid at a single melting point. The typical mesophases which can intermediately exist between crystal and isotropic liquid are known as liquid crystals and plastic crystals.[1–3] The former are composed of elongated rod-like or lath-like shape of molecules, whereas molecules in the latter are roughly of globular shape. Recently Chandrasekhar *et al.*[4] reported the

† Present address: Department of Chemistry, School of Science, Kwansei Gakuin University, Nishinomiya 662, Japan.

first observation of the third class of intermediate phase in pure, single-component systems of relatively simple plate-like or disc-like molecules. They found evidence, in certain benzene-hexa-*n*-alkanoates, for a lamellar-type mesophase, having a structure in which the molecular discs are stacked, with irregular spacings, in hexagonally arranged columns. The structure has translational periodicity in two dimensions but liquid-like disorder in three dimensions. They designate this new state of matter as "disc-like mesophase." Similar mesogens having a triphenylene core have also been found by French groups.[5–11] The intermediate state is called "discotic mesophase."

The report by Chandrasekhar *et al.*[4] motivated us to investigate this new class of mesophase from a thermodynamic point of view. We measured precisely the heat capacities of benzene-hexa-*n*-hexanoate, $C_6(OCOC_5H_{11})_6$ (Figure 1: abbreviated hereafter as BHn-hexanoate)[4] between 13 and 393 K and found two new phase transitions at 251.58 and 291.46 K in addition to two higher temperature transitions at 348.27 and 368.74 K. For this compound Chandrasekhar *et al.*[4] found a mesophase between 341.5 and 359.2 K based on thermal analyses. However, they revised[12] quite recently their old data[4] and found a "solid" phase between 348.9 and 367.7 K instead of "the mesophase." This conclusion accords well with our calorimetric results. Therefore, the present paper will be concerned not with thermodynamic study of the new mesophase itself but with that of its precursor compound.

The enthalpy and entropy of transitions will be estimated in section 4 and the four phase transitions will be treated as a kind of successive phase transitions. The infrared spectra remarkably depend on temperature. Relationship between the infrared spectra and molecular motions will be described in section 5. In section 6 we shall discuss the nature of the highest temperature "solid" phase.

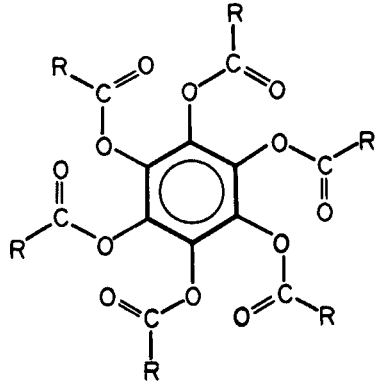

FIGURE 1 Molecular formula of benzene-hexa-*n*-alkanoate. $C_6(OCOC_5H_{11})_6$: R being -*n*-C_5H_{11}.

2 EXPERIMENTAL

Sample preparation

The compound $C_6(OCOC_5H_{11})_6$ was synthesized from inositol (Nakarai Chemicals, Ltd.: Extra Pure Reagent) and *n*-caproylchloride (Tokyo Kasei Kogyo Co., Ltd.: Extra Pure Reagent) by the published methods.[13–15] The crude material was recrystallized four times from absolute ethanol to give needle crystals and dried for 24 hours in a vacuum.
Anal. Calcd. for $C_{42}H_{66}O_{12}$: C, 66.12%; H, 8.72%. Found: C, 65.96%; H, 8.70%.

Heat capacity measurements

The heat capacities were measured with an adiabatic calorimeter[16] between 13 and 393 K. A calorimeter cell made of gold and platinum contained 18.0162 g ($\triangleq$ 0.0236131 mol) of the compound and a small amount of helium gas to aid the heat transfer. A platinum resistance thermometer (Leeds & Northrup Co., Ltd.) used in this experiment has been calibrated based on the IPTS–68 temperature scale.

Infrared and far infrared spectroscopy

Spectra in the range 4000–400 cm^{-1} were recorded for Nujol mulls and KBr disc with an Infrared Spectrophotometer Model DS–402G (Japan Spectroscopic Co., Ltd.) and far infrared spectra in the range 400–30 cm^{-1} with a Far Infrared Spectrophotometer Model FIS–3 (Hitachi, Ltd.) between 100 and 383 K.

Polarizing microscopy

Textures of the phases above room temperature were observed by a Polarizing Microscope Model BHA–751–P (Olympus) equipped with a heating stage (Union Optical Co., Ltd., Model CMS-2). Temperature of the specimen was monitored by a chromel-P *versus* constantan thermocouple.

3 RESULTS

The results of the heat capacity measurements for BHn-hexanoate in the whole temperature region investigated are listed in Table I and plotted in Figure 2. Standard thermodynamic functions are summarized in Table II. Four phase transitions were observed at 251.58, 291.46, 348.27 and 368.74 K.

TABLE I

Molar heat capacity of $C_6(OCOC_5H_{11})_6$: molecular weight 762.976

T/K	C_p/J K^{-1} mol^{-1}	T/K	C_p/J K^{-1} mol^{-1}	T/K	C_p/J K^{-1} mol^{-1}
12.235	15.521	117.715	542.78	287.286	1498.6
14.222	23.770	122.156	557.46	289.737	1691.8
14.886	27.396	126.070	570.78	291.456	1937.6
15.925	32.095	130.395	584.63	292.616	1569.4
17.224	38.521	134.749	598.95	293.896	1395.4
18.502	45.152	138.665	610.80	295.238	1328.9
19.805	52.213	143.000	624.95	296.841	1302.0
21.158	60.423	147.415	638.43	299.153	1289.3
22.560	69.105	151.985	653.11	301.931	1289.2
24.087	78.599	156.679	668.03	305.317	1291.0
25.660	88.271	161.513	683.80	308.634	1298.6
27.141	98.058	166.405	699.54	312.105	1310.9
28.592	107.71	171.309	716.24	316.137	1322.7
30.066	117.54	176.257	732.73	319.906	1334.9
31.593	127.70	180.671	749.31	324.154	1349.8
33.438	140.04	185.600	767.19	328.533	1365.1
35.483	153.84	190.488	786.20	332.877	1380.8
37.401	166.45	195.334	806.13	337.183	1398.3
39.263	178.74	200.139	827.14	342.129	1417.1
41.518	192.96	204.911	849.53	345.654	1435.9
44.080	208.89	209.636	873.67	347.983	4541.9
46.507	223.49	213.767	897.37	348.271	177450.0
48.475	234.80	218.337	926.58	348.306	100580.0
49.483	240.82	222.817	959.12	348.398	32329.0
50.947	249.66	227.197	998.85	349.163	2284.7
52.576	259.39	231.472	1045.1	350.791	1403.7
54.360	269.96	235.627	1104.5	353.503	1408.1
56.170	280.95	239.637	1184.4	358.796	1417.0
58.007	291.30	243.055	1280.7	360.681	1424.3
59.898	302.32	245.885	1413.8	362.878	1433.0
61.761	311.62	248.520	1627.1	365.067	1441.0
63.612	321.46	250.530	2153.3	367.214	1527.8
65.402	330.69	251.402	18160.0	368.475	12524.0
67.209	339.44	251.555	78829.0	368.713	166410.0
69.034	349.09	251.619	67192.0	368.734	816570.0
70.808	357.87	251.796	15694.0	368.739	2941600.0
72.703	366.44	252.736	1983.3	368.742	1429700.0
74.718	376.04	254.577	1276.5	368.752	289580.0
76.742	384.77	256.677	1247.8	371.898	1598.3
78.777	394.40	260.516	1255.1	374.800	1600.4
80.930	403.73	262.893	1264.6	378.823	1602.6
83.113	413.22	264.315	1268.6	383.429	1605.8
85.567	423.31	265.256	1275.8	388.023	1609.1
88.276	434.82	266.674	1283.9	391.842	1610.4
91.070	445.88	267.605	1288.5		
93.796	456.96	269.103	1297.0	Supercooled Phase III	
96.636	467.86	273.921	1321.3	254.637	1223.5
100.318	481.81	276.666	1341.5	257.467	1233.7
104.677	497.81	279.382	1364.6	260.908	1248.2
109.013	513.16	282.064	1393.5	264.809	1271.1
113.337	528.22	284.705	1432.3	268.834	1291.8
				272.807	1316.4

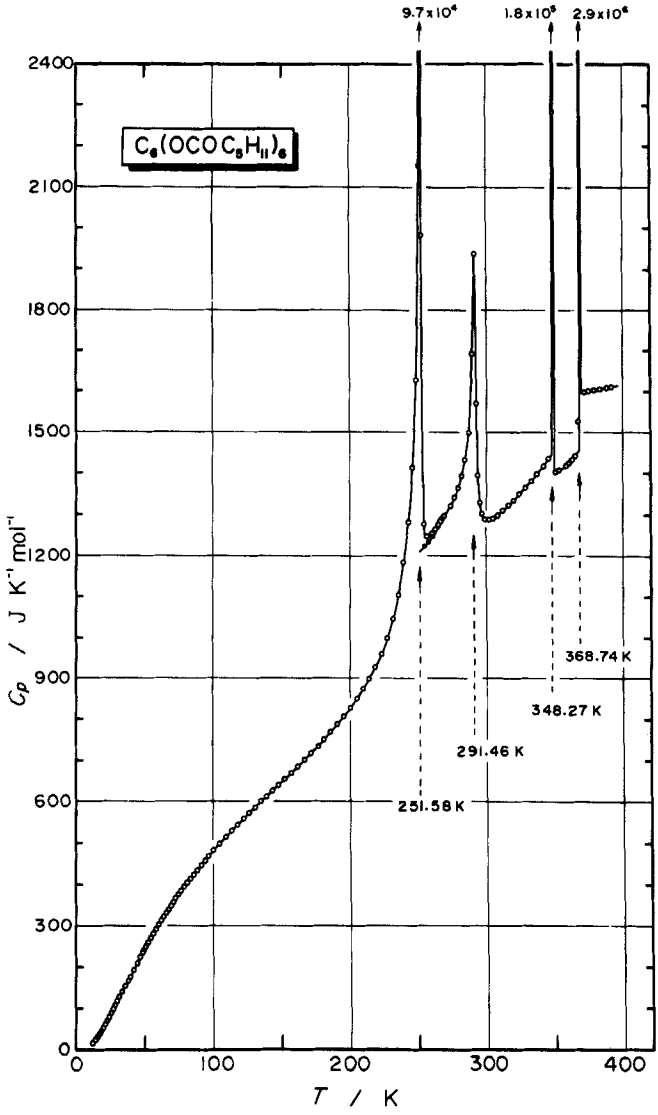

FIGURE 2 Molar heat capacity of $C_6(OCOC_5H_{11})_6$. Solid circles correspond to the heat capacities in the undercooled region.

TABLE II

Standard thermodynamic functions for $C_6(OCOC_5H_{11})_6$ in J K^{-1} mol^{-1}

T/K	C_p°	S_T°	$(H_T^\circ - H_0^\circ)/T$	$-(G_T^\circ - H_0^\circ)/T$
5	1.37	0.458	0.344	0.114
10	9.94	3.518	2.618	0.900
20	53.33	21.983	15.896	6.087
30	117.10	55.420	38.821	16.599
40	183.38	98.233	66.709	31.524
50	243.94	145.75	96.181	49.573
60	302.82	195.50	125.82	69.683
70	353.87	246.02	154.72	91.307
80	399.70	296.30	182.51	113.79
90	441.65	345.83	209.02	136.82
100	480.60	394.39	234.33	160.06
120	550.33	488.35	281.25	207.10
140	615.16	578.11	324.42	253.69
160	678.87	664.39	364.73	299.66
180	746.79	748.17	403.34	344.83
200	826.51	830.82	441.52	389.30
220	938.66	914.41	481.16	433.24
240	1193.2	1004.8	527.80	477.00
	Phase Transition (IV → III) at 251.58 K			
260	1253.5	1190.3	665.93	524.27
280	1370.5	1286.8	711.45	575.37
	Phase Transition (III → II) at 291.46 K			
298.15	1294.8	1380.0	758.49	621.56
300	1289.3	1388.0	761.76	626.26
320	1335.3	1472.3	795.80	676.49
340	1409.0	1555.4	829.61	725.78
	Phase Transition (II → I) at 348.27 K			
360	1421.6	1682.7	907.02	775.63
	Phase Transition (I → Liquid) at 368.74 K			
380	1603.4	1856.1	1027.9	828.19
390	1610.2	1897.9	1042.8	855.10

TABLE III

Fractional melting of $C_6(OCOC_5H_{11})_6$

T/K	f	$1/f$
368.7304	0.32715	3.0567
368.7377	0.50499	1.9802
368.7397	0.68298	1.4642
368.7438	0.86061	1.1620

triple point of sample	368.7440 K
triple point of pure material	368.7507 K
purity of sample	99.98 mole%

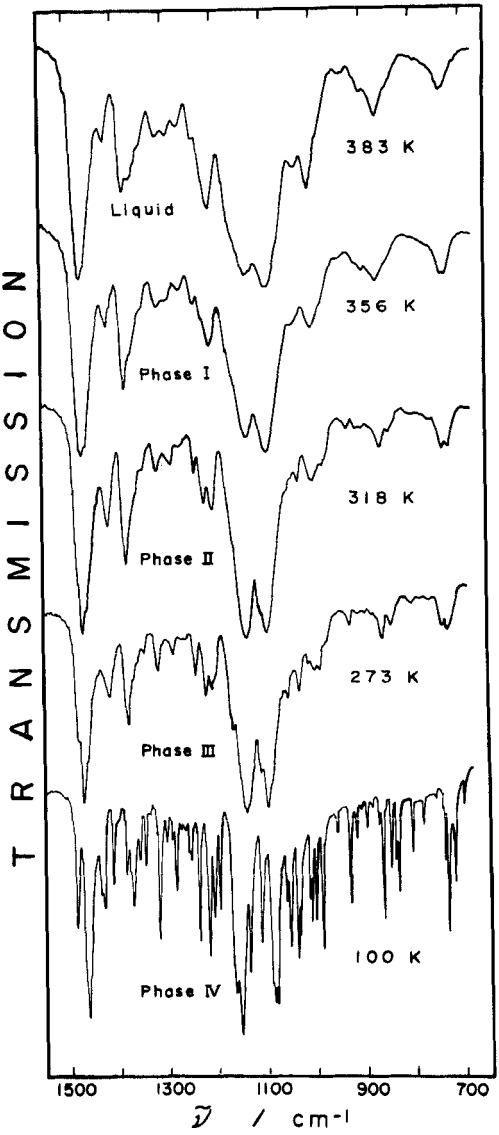

FIGURE 3 Infrared spectra of $C_6(OCOC_5H_{11})_6$.

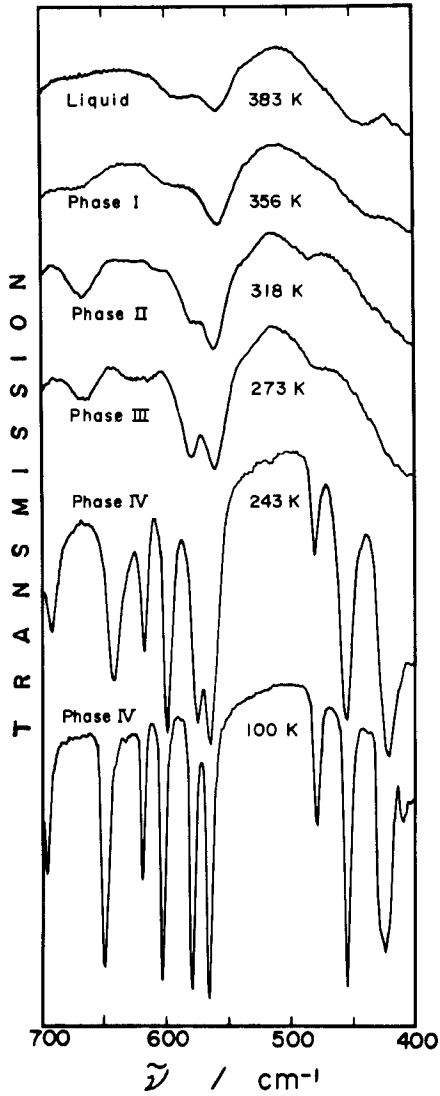

FIGURE 4 Infrared spectra of $C_6(OCOC_5H_{11})_6$.

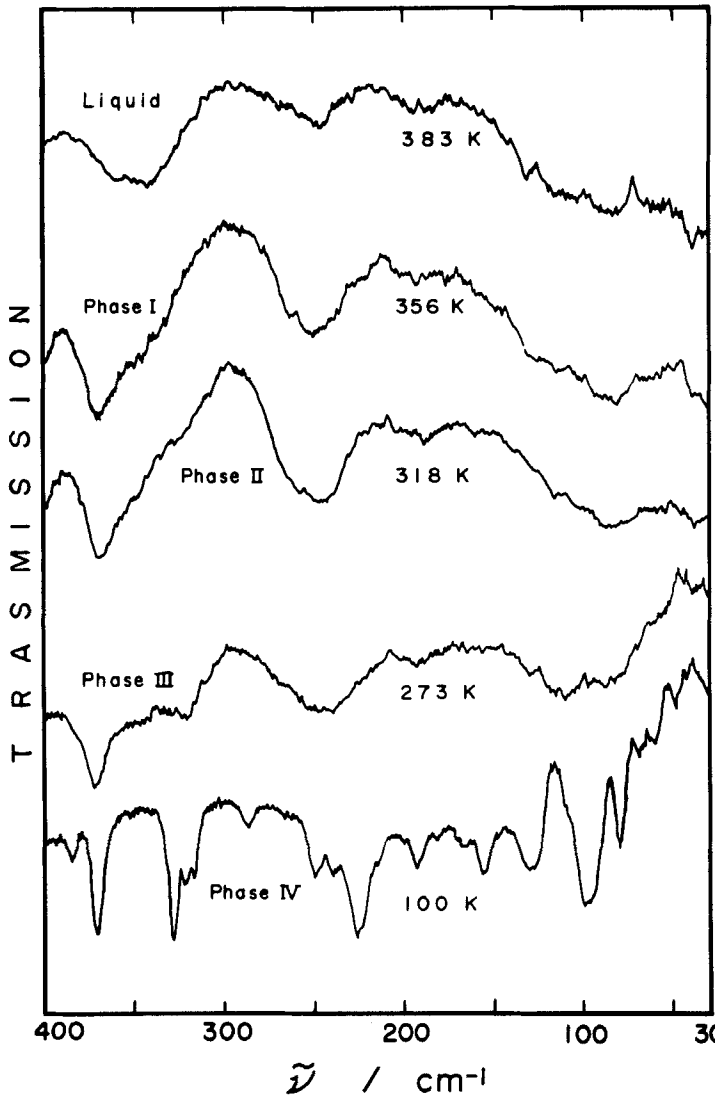

FIGURE 5 Far infrared spectra of $C_6(OCOC_5H_{11})_6$.

(a)

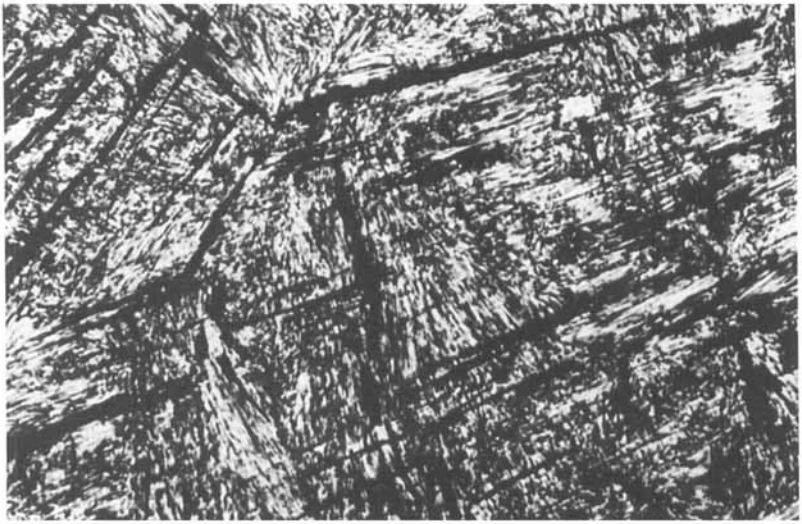

(b)

FIGURE 6 The optical texture of Phase I (a), Phase II (b), Phase III (c) on cooling and Phase I (d) on heating. Many cracks appear in Phase II. Crossed polarizers, magnification: 400× for (a), (b) and (d), and 100× for (c).

(c)

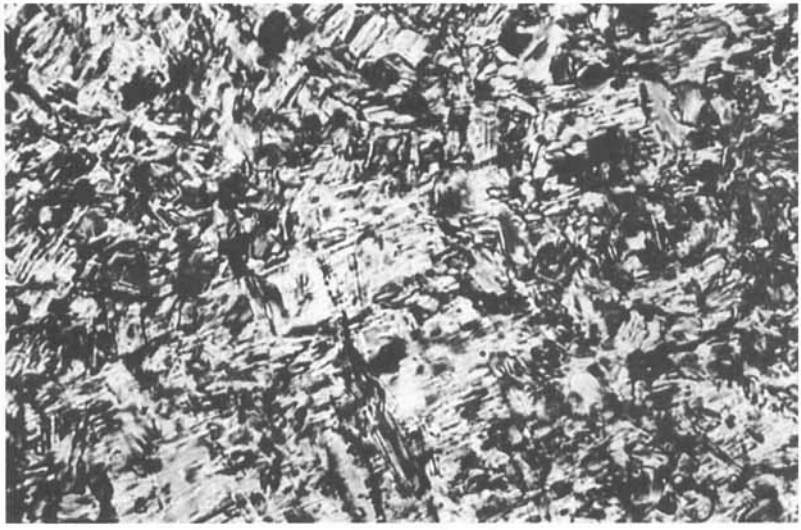

(d)

Of these four the two lower temperature transitions were newly found in this study. The temperatures of the two higher temperature transitions accord well with the recent revised data (348.9 and 367.7 K) by Chandrasekhar *et al.*[12] At the highest transition temperature the compound is transformed from a "solid" state to an isotropic liquid.

Thermal equilibrium after an energy input was normally attained within 20 min except for the regions in the vicinity of phase transitions, where equilibration time were considerably elongated. It is interesting, however, that equilibrium in fusion was attained within only one hour in contrast to very long equilibration times encountered for usual fusion processes.

In what follows, the four solid phases are designated as Phases I, II, III and IV, respectively, in going from high to low temperatures. The phase transitions at 348.27 and 368.74 K are characteristic of typical first-order while the transition at 291.46 K bears a higher-order nature. Although the transition from Phase IV to Phase III apparently seems in Figure 2 to be of higher-order, this phase transition has a large amount of first-order component in the vicinity of the transition point. This situation will become clear in the next section dealing with the transition entropy. Phase III was easily undercooled, the heat capacities of the undercooled state being shown in Figure 2 by solid circles.

The purity of the sample was determined by a fractional fusion method (Table III). Plot of the reciprocal of the fraction melted (f) against the melting temperature (T) gave a straight line, indicating nonexistence of solid-soluble impurities, and the slope yielded a sample purity of 99.98 mole per cent. The triple point of pure material was 368.75 K.

Infrared and far infrared spectra recorded for Nujol mulls at all phases are reproduced in Figures 3, 4 and 5. Absorption bands observed above 1500 cm^{-1} were only the C—H and C=O stretching modes in the ranges 2950–2850 cm^{-1} and 1775–1757 cm^{-1}, respectively. The absorption spectra obtained for KBr disc were identical with those shown in these figures.

The transitions could be seen very clearly through a polarizing microscope both on cooling and on heating. When the sample was cooled from the isotropic liquid to Phase I, fine needle-like texture appeared (Figure 6(a)). At the transition point in going from Phase I to Phase II, the optical view changed to tiny mosaic and simultaneously a marked contraction of volume induced to generate many cracks (Figure 6(b)). On further cooling, a change in the texture was observed at the transition temperature from Phase II to Phase III (Figure (c)). On the other hand, when the sample in Phase II was heated to Phase I, the cracks adhered together at the transition point to give a quite different texture of Phase I (Figure 6(d)) compared with that in Figure 6(a). These changes in texture were reproducible on every temperature cycling.

4 ENTHALPY AND ENTROPY OF PHASE TRANSITION

To separate the excess heat capacities due to phase transitions from the observed values, we adopted here an effective frequency distribution method described previously.[17] Normal heat capacity principally consists of the contributions from a continuous phonon distribution and many discrete intramolecular vibrational modes. The latter contribution can be well approximated by the Einstein model. A borderline between the continuous and discontinuous frequency distributions was assumed here to be located at 700 cm^{-1}. Since the present molecule consists of 120 atoms, the number of degrees of freedom for a molecule is 360. Among them, thirteen modes of intramolecular vibration (138 degrees of freedom) were reasonably assigned base on the infrared spectra and twenty nine modes (174 degrees of freedom) were tentatively assigned. The contribution of these modes to the heat capacity was calculated in the Einstein approximation. The contribution from the rest of degrees of freedom was effectively included to a continuous spectrum.[17] By using 58 C_p values between 14.222 and 147.415 K the "best" effective frequency distribution below 700 cm^{-1} was determined through a computer-fitting. The continuous spectrum thus obtained consists of two Debye-type distributions ($G(\tilde{\nu}) = 0.6938 \times 10^{-4}\tilde{\nu}^2$, $0-45$ cm^{-1}; $G(\tilde{\nu}) = 0.1517 \times 10^{-3}\,\tilde{\nu}^2$, $45 - 100$ cm^{-1}) and three constant distributions ($G(\tilde{\nu}) = 0.2717$, $100-300$ cm^{-1}; $G(\tilde{\nu}) = 0.6004 \times 10^{-1}$, $300-500$ cm^{-1}; $G(\tilde{\nu}) = 0.1350$, $500 - 700$ cm^{-1}). This method was able to reproduce the experimental C_p values in this temperature region within a root-mean-square deviation of ± 0.433 J K^{-1} mol^{-1}. The extrapolation of C_p values above 147.5 K is drawn by broken lines A and C in Figure 7. This extrapolated curve, though rather accidental, coincides smoothly with the C_p values of Phase I. Moreover, since the slope of C_p *versus* T curve in Phase I is practically identical with that in Phase II, we simply lifted curve C by 59.86 J K^{-1} mol^{-1} to obtain curve B. Curves A and C were adopted to represent "normal" heat capacities for Phases IV and I, respectively, while curve B was used for both Phases III and II.

Figure 8 shows the excess heat capacities due to phase transitions and fusion thus obtained. Since the two lower temperature transitions are overlapped, it is difficult to distribute unambiguously the relevant thermodynamic quantities between these two. A possible partition will be made as follows. As was mentioned in Section 3, the lowest temperature transition is fundamentally characterized by a first-order nature. Therefore, we considered that the pretransitional effect appearing from 170 K may be associated with not the lowest but the second lowest temperature transition. This kind of assumption may be reasonable if two phenomena take place independently. A hypothetical excess heat capacity ΔC_p of Phase III was assumed to be

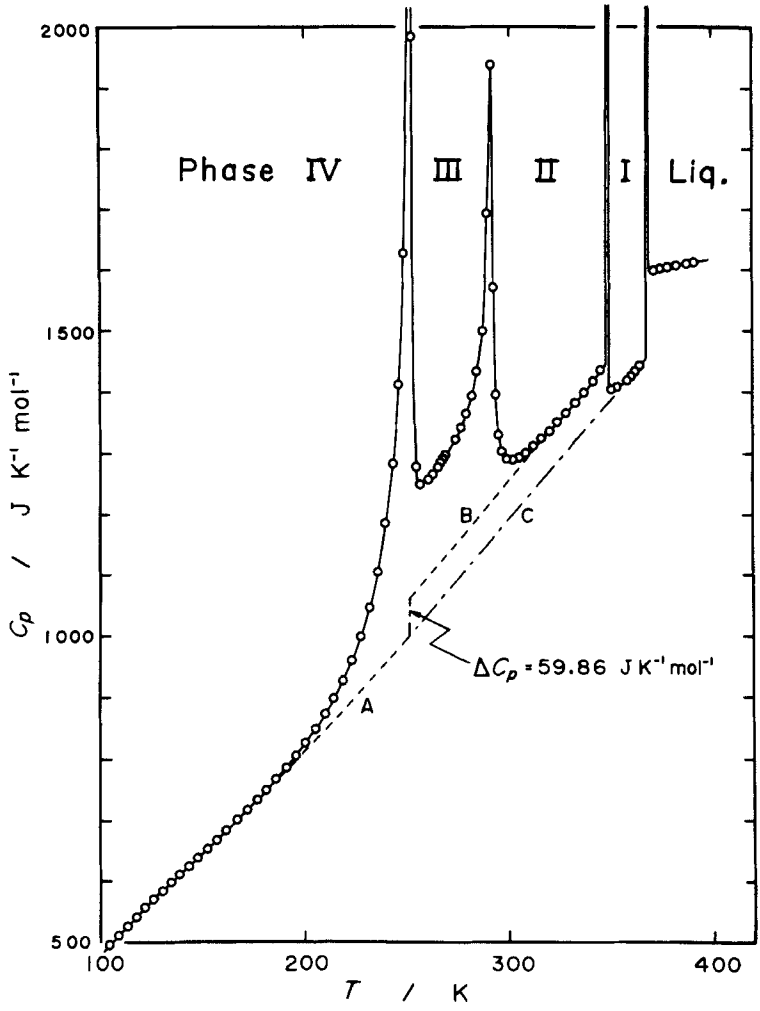

FIGURE 7 Separation of the excess heat capacities due to phase transitions from the experimental values. Broken lines A and B represent the "normal" heat capacities. Line C is a simple extension of Curve A.

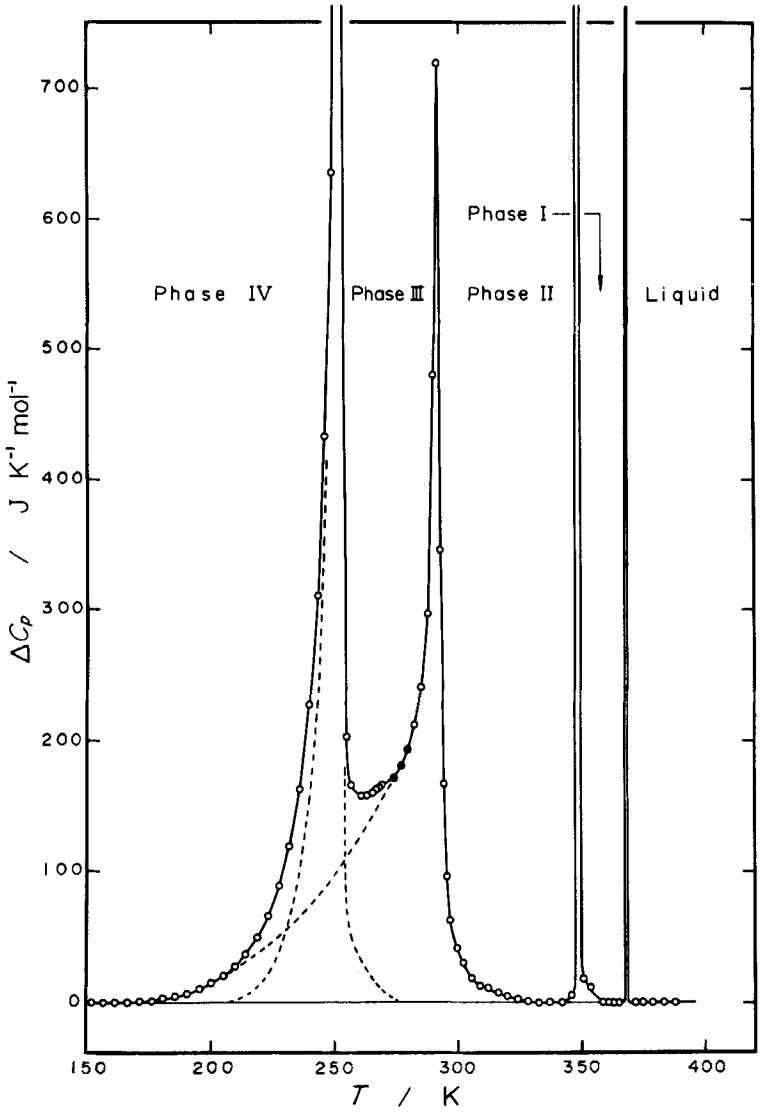

FIGURE 8 Excess heat capacities due to phase transitions. Separation of two lower temperature transitions was made by using three points shown by solid circles (see text).

represented by the following equation[18] if the lowest temperature transition would not interfere:

$$\Delta C_p = A \exp\left(\frac{-B}{RT}\right) T^2 \tag{1}$$

or

$$\ln\left(\frac{T^2 \Delta C_p}{\text{J K mol}^{-1}}\right) = C - \frac{B}{RT}, \tag{2}$$

where A, B and C are adjustable parameters and R is the gas constant. Three ΔC_p values at 273.921, 276.666 and 279.382 K, shown by solid circles in Figure 8, were substituted in Eq. (2). These three points lie on a straight line in a $\ln(T^2 \Delta C_p)$ *versus* $1/T$ diagram. The slope and the intercept at $1/T = 0$ gave $B = 17.88$ kJ mol^{-1} and $C = 24.22$ ($A = \exp(C)$). A broken line followed by three solid circles in Figure 8 indicates the excess heat capacity curve calculated from Eq. (1). This extrapolation curve also fitted well to the experimental ΔC_p below 210 K. The excess heat capacities due to the lowest temperature transition were determined by subtracting the quantity of Eq. (1) from the observed ΔC_p to give broken lines in Figure 8.

The enthalpy and entropy of transition were determined by combining the ΔC_p shown in Figure 8 and independent enthalpy measurements for each phase transition. Table IV summarizes these data and Figure 9 represents the temperature dependence of the entropy acquisition. A first-order character of the lowest temperature transition is apparent in this figure.

The present molecule consists of a $C_6(OCO—)_6$ core and six *n*-paraffin moieties, $6(\text{-}n\text{-}C_5H_{11})$. We propose that the phase transitions in the solid are mainly associated with successively increasing conformational disorder in paraffinic chains attained through gauche-trans-type kinking,[19] whereas the fusion is mainly concerned with positional and orientational disordering processes of molecules as a whole. If the sequential solid-solid phase transitions are considered as partial meltings, the total entropy of "fusion" must be considered as being the cumulative entropy of fusion and transi-

TABLE IV

Enthalpy and entropy of phase transitions in $C_6(OCOC_5H_{11})_6$

Transition	T_c/K	ΔH/kJ mol^{-1}		ΔS/J K^{-1} mol^{-1}	
Phase IV → Phase III	251.58	(25.66)	37.93	(102.67)	148.78
Phase III → Phase II	291.46	(12.27)		(46.11)	
Phase II → Phase I	348.27	16.26		46.68	
Phase I → Liquid	368.74	33.50		90.86	
			total	286.32	

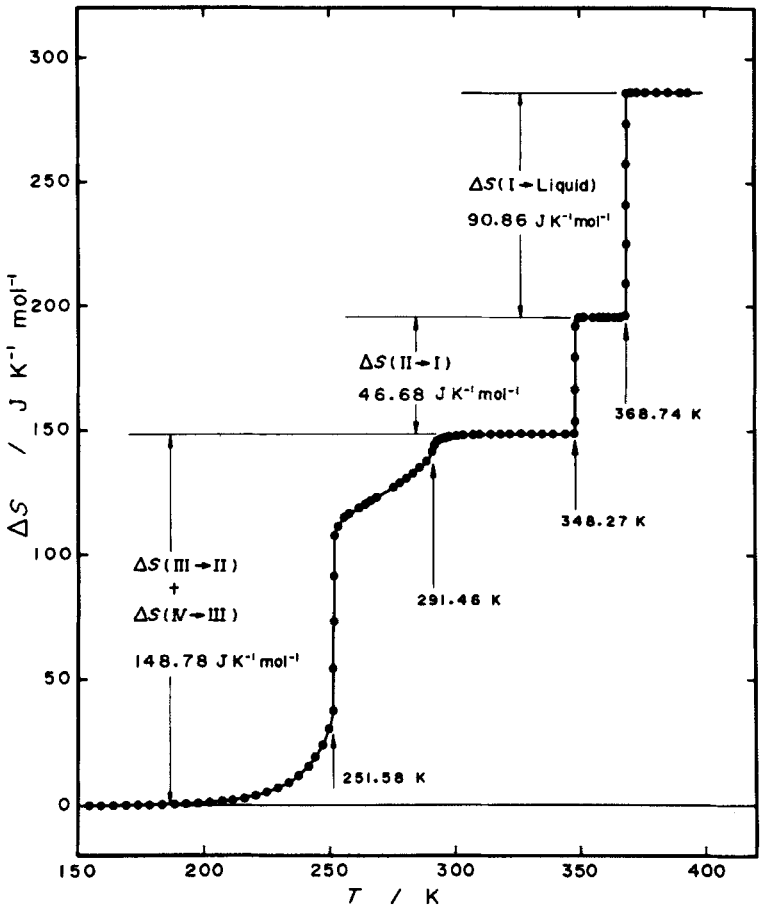

FIGURE 9 The temperature dependence of the entropy acquisition due to phase transitions and melting for $C_6(OCOC_5H_{11})_6$.

tions.[3] In the present case the sum of entropy changes, ΔS_{total}, amounts to 286.32 J K^{-1} mol^{-1}. To account for this value, we regarded the total entropy as consisting of the following three components:

$$\Delta S_{total} = \Delta S\{C_6(OCO—)_6\} + 24\Delta S(—CH_2—) + 6\Delta S(—CH_3), \quad (3)$$

where the first term in the right-hand-side of equation represents the entropy change arising from positional and rotational disorder of a "rigid" core, the second term an entropy gain due to the available conformations of methylene groups and the last term from an entropy increase due to methyl groups. Since, from the analogy of the molecular structure of 1,4-dimethoxybenzene,[20] the $C_6(OCO—)_6$ core may be regarded as being planar and

"rigid" over the whole temperature region investigated here, we shall replace $\Delta S\{C_6(OCO—)_6\}$ by an averaged value of the entropy of fusion for benzene (35.4 J K^{-1} mol^{-1})[21] and that for hexafluorobenzene (41.6 J K^{-1} mol^{-1})[22]:

$$\frac{\Delta S\{C_6(OCO—)_6\}}{J\,K^{-1}\,mol^{-1}} = 38.5 \pm 3.1. \tag{4}$$

The contribution of $6\Delta S(-CH_3)$ can be attributed to the excess entropy possessed by hexamethylbenzene beyond the melting entropy of benzene core given by Eq. (4). Hexamethylbenzene crystal exhibits two solid-solid phase transitions at 116.48 and 383.65 K as well as a fusion at 438.5 K. The entropy changes for these transitions are determined by several workers[23–26]: the averaged values are 9.54, 4.71 and 46.96 J K^{-1} mol^{-1}, respectively, and the sum amounts to 61.2 J K^{-1} mol^{-1};

$$\frac{6\Delta S(—CH_3)}{J\,K^{-1}\,mol^{-1}} = 61.2 - 38.5 = 22.7. \tag{5}$$

On the other hand, the value of $\Delta S(—CH_2—)$ can be estimated from the calorimetric measurements for normal paraffins.[27–31] The total entropy change due to melting and solid-solid phase transition, if it exists, is plotted in Figure 10 against the carbon number n of normal paraffins for the range $4 \leqq n \leqq 20$. When n is even, the total entropy change is given by ΔS/J K^{-1} mol^{-1} = $9.47 + 10.84_6 n \pm 0.64$, whereas for odd n, ΔS/J K^{-1} mol^{-1} = $10.24 + 9.78_0 n \pm 0.79$. The entropy increment per methylene group, $\Delta S(—CH_2—)$, is given by the averaged slope of these two straight lines:

$$\frac{\Delta S(—CH_2—)}{J\,K^{-1}\,mol^{-1}} = 10.31_3 \pm 0.53_3. \tag{6}$$

This value is very close to $R\ln 3$ (=9.13 J K^{-1} mol^{-1}) as is expected from the fact that the number of different conformations of a methylene group around C—C bond is three. The small difference between them can be attributed to the entropy gain associated with a volume expansion.[32] Since six paraffinic chains are equivalent in the present molecule, it is convenient to treat $24\Delta S(—CH_2—)$ as a unit of $6\Delta S(—CH_2—)$:

$$\frac{6\Delta S(—CH_2—)}{J\,K^{-1}\,mol^{-1}} = 61.9 \pm 3.2. \tag{7}$$

Accordingly, the total entropy change for the present material is expected to be

$$\begin{aligned}\frac{\Delta S_{total}}{J\,K^{-1}\,mol^{-1}} &= (38.5 \pm 3.1) + (61.9 \pm 3.2) \times 4 + 22.7 \\ &= 308.8 \pm 15.9.\end{aligned} \tag{8}$$

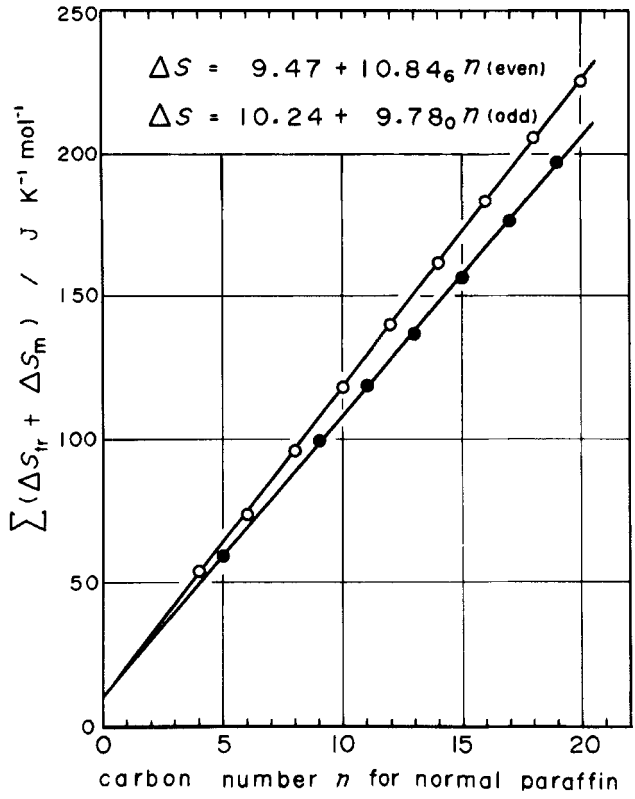

FIGURE 10 The total entropy change due to phase transition and melting for normal paraffins (○; for even n, ●; for odd n). The values are taken from references.[27–31]

The observed value of 286.32 J K^{-1} mol^{-1} can be well accounted for by this model-calculation if we keep in mind the fact that in the real molecule all the configurations cannot necessarily be realized because of steric hindrances and thus the model-calculation is somewhat overestimated. At any rate, as far as the entropy is concerned, a disc-like molecule of $C_6(OCOC_5H_{11})_6$ acquires almost full number of its available configurations in a liquid state through successive phase transitions.

In passing, it should be noticed here that, although the cumulative entropy can theoretically be computed for simple molecules,[33] it has been only semi-empirically estimated for large molecules.[34–37] Blasenbrey and Pechhold[19] reported a kink-block theory to interpret the melting and transitions in n-paraffins. This treatment, however, cannot be directly applied to the present case, because six paraffinic chains are bounded to the central $C_6(OCO—)_6$ core and their gauche-trans-type kinking is not completely realized.

Now that the total entropy of melting and solid-solid phase transitions has been fairly well accounted for by the semi-empirical method described above, we shall next discuss possible mechanisms of the particular phase transitions. For convenience, five carbon atoms in a single paraffinic chain will be numbered in turn from the outermost to the innermost carbon: *e.g.* C(1) atom corresponds to the methyl carbon and C(5) to the innermost methylene carbon. As shown in Figure 9, the sum of transition entropies of ΔS(IV → III) and ΔS(III → II) is 148.78 J K^{-1} mol^{-1}, and this value is practically the same as the sum of $6\Delta S(-CH_3) + 6\Delta S(-CH_2-) \times 2 = (146.5 \pm 6.4)$ J K^{-1} mol^{-1}. Moreover, the entropy change of ΔS(II → I) = 46.68 J K^{-1} mol^{-1} has roughly the same order of $6\Delta S(-CH_2-) = (61.9 \pm 3.2)$ J K^{-1} mol^{-1} and the ΔS(I → liquid) = 90.86 J K^{-1} mol^{-1} corresponds to a sum of $6\Delta S(-CH_2-) + \Delta S\{C_6(OCO-)_6\} = (100.4 \pm 6.3)$ J K^{-1} mol^{-1}. From these correspondences, we can draw a picture concerning the mechanisms of phase transitions as follows. In the lowest temperature phase (Phase IV) all the molecules are regularly arranged and a molecule has a structure with fully extended paraffinic chains. On heating, molecular motions are gradually excited, especially the reorientational motion of methyl groups appears as the pretransitional effect. In passing over to Phase II, the C(1) methyl group and the C(2) and C(3) methylene groups attain their full disorder through gauche-trans-type kinking. At the transition from Phase II to Phase I, the C(4) methylene group acquires its motional freedoms. Finally at fusion the innermost C(5) methylene group attains the full number of conformations and at the same time the $C_6(OCO-)_6$ core melts. In other words, the conformational melting proceeds from the periphery of a molecule into its inside core by giving rise to a phase transition in each stage. This model for the present successive phase transitions is speculative and NMR or X-ray analysis is needed to test it.

5 INFRARED SPECTRA AND MOLECULAR MOTION

Infrared and far infrared spectra of the present compound remarkably depend on temperature in the whole wavenumber region studied here (Figures 3, 4 and 5). One of the noticeable changes is a smearing effect of the intramolecular vibrational modes with increasing temperature in the range between 1550 and 700 cm^{-1} (Figure 3). The vibrational modes appearing in this wavenumber region mainly originate in the paraffinic chains. In the lowest temperature phase (Phase IV) the absorption bands are well resolved: molecular motions being suppressed and molecules being arranged in an ordered state. These absorption bands become broader and more smeared when the crystal undergoes the successive phase transitions. The spectrum recorded at Phase I bears a close resemblance to that

at the liquid state. This situation is also encountered in the spectra in the range from 700 to 400 cm^{-1} (Figure 4). This fact suggests Phase I being a highly disordered condensed state as is predicted from the consideration of the transition entropies. The smearing effect can be, therefore, accounted for by either rapid motions of the paraffinic chains (the vibrational and rotational relaxations) or by distribution of the force-fields of the particular vibrational modes arising from different conformations.

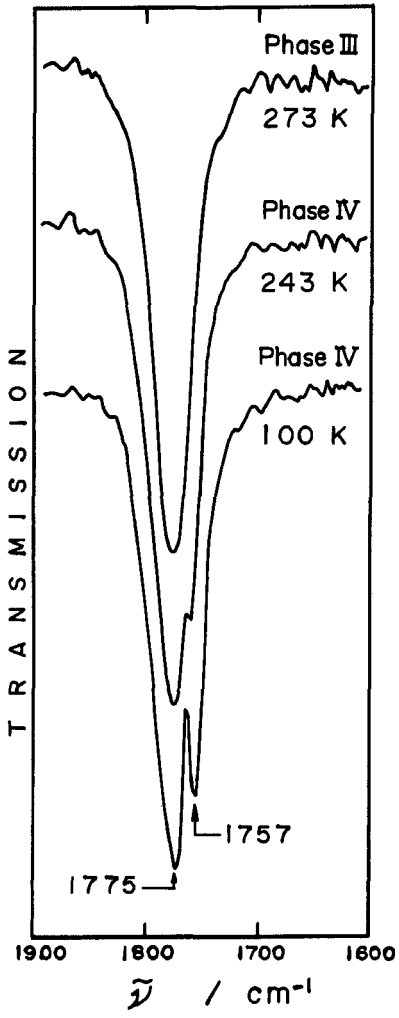

FIGURE 11 Temperature dependence of the C=O stretching band for $C_6(OCOC_5H_{11})_6$.

Another noticeable point is a change in the crystal symmetry in which a molecule is located. This effect can be seen in the lower wavenumber region (Figures 4 and 5) where intermolecular lattice vibrations are observable. The number of infrared active bands are remarkably reduced in progression of phase transitions, especially when the crystalline phase is transformed from Phase IV to Phase III.

In passing, it should be noticed here that the strong C=O stretching band at 1775 cm^{-1} splits into doublet (1775/1757 cm^{-1}) with unequal intensities in Phase IV (Figure 11). As shown in Figure 12, the most probable molecular structure having fully extended paraffinic chains may be a configuration characterized by C_{6h} or S_6 symmetry. If one of these configurations were realized in the fully ordered phase (Phase IV), the C=O stretching mode would give a single peak. But it is not the case. Therefore there exists a possibility that the molecules are somewhat distorted in Phase IV and have no higher symmetry than C_{6h} or S_6. Alternate possibility of the split C=O band in Phase IV may be that the unit cell structure is such that there are

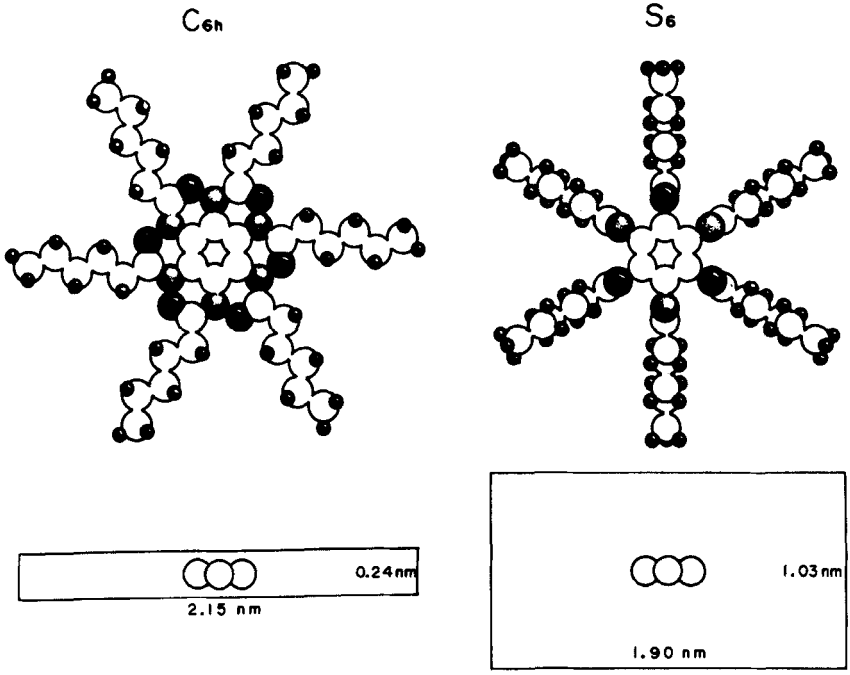

FIGURE 12 Possible molecular structures of $C_6(OCOC_5H_{11})_6$ having fully extended paraffinic chains. Side-views are also drawn schematically: the benzene core is shown by three open circles.

two molecules per unit cell. In this case the splitting could be a crystal field splitting while the molecules indeed have C_{6h} or S_6 symmetry. The magnitude of the observed splitting (*ca.* 18 cm^{-1}) is typical of crystal field effects.

6 AS TO THE HIGHEST TEMPERATURE "SOLID" PHASE

From the nature of X-ray diffraction pattern and the observation of optical textures, Chandrasekhar *et al.*[4,12] have concluded that the mesophase found for some BHn-alkonoates is not a plastic crystal but a highly ordered lamellar type of liquid crystal. Their observation of the mesophase textures under a polarizing microscope showed often a broken-fan texture similar to that of smectic C, occasionally with striations running across the fans as in smectic E and F, and sometimes flower-like particles. Phase I displays quite different textures on cooling and on heating (Figures 6(a) and (d)). Neither of these two textures corresponds to any of those reported for the disc-like mesogens by Chandrasekhar *et al.*[4] The present textures seem to be of crystal rather than of liquid crystal; confirming the assessment of Chandrasekhar *et al.*[12]

We shall next consider a possibility of Phase I being a plastic crystal. The concept of plastic crystals was recognized first by Timmermans[38] based on two criteria, one on thermodynamic, the other on structural grounds. He noted that plastic crystals exhibit a low entropy of fusion, and he proposed an arbitrary but convenient upper limit of $\Delta S_m = 21$ J K^{-1} mol^{-1}. This value is satisfactory in most cases, although some exceptions are known even in simple molecules.[39] The melting entropy of 90.86 J K^{-1} mol^{-1} found for the present compound is apparently far beyond the Timmermans thermodynamic criterion. However, it should be remarked that the melting entropy is very small if we compare it with the total entropy change of 286.32 J K^{-1} mol^{-1}. On the other hand, if the molecules in Phase I had disc-like or plate-like structure as shown in Figure 12, such a structure would surely violate the structural criterion for plastic crystals.[38,39] But, as can be understood from the large amount of the cumulative transition entropy, it is certainly true that real molecules are very flexible and more globular than the disc-like structure with C_{6h} symmetry at least in Phase I. According to the X-ray study by Chandrasekhar *et al.*[4], the mean intermolecular spacing along hexagonal axis is *ca.* 0.6 nm in both Phases I and II; much longer than the static molecular thickness of 0.24 nm. This fact confirms the picture of conformational melting of the paraffinic chains discussed in Section 4. Although the low melting entropy and the more globular molecular structure in Phase I favor the aspect of plastic crystals, the present material does not necessarily seem to have other properties characteristic of plastic crystals.[2] In this sense, we cannot simply regard Phase I as being a plastic crystal.

As was discussed in Section 5, the infrared and far infrared spectra of Phase I bear a close resemblance to those of the isotropic liquid. This fact suggests that molecular motions in Phase I, especially those of the paraffinic chains, are highly excited. Therefore, we incline to conclude that the highest temperature "solid" phase of $C_6(OCOC_5H_{11})_6$ is a crystalline phase, as Chandrasekhar *et al.*[12] have reported in their revised paper. Strictly speaking, Phase I is a highly disordered crystalline phase, in which conformational melting of the paraffinic chains does proceed to a great extent. To understand more closely the nature of Phase I, it would be useful to compare the thermodynamic properties of the present substance with those of the homologous series, which really exhibit the new class of mesophase. Such a study is now in progress.

Acknowledgements

The authors express their sincere thanks to Itoh Science Foundation for supplying them a polarizing microscope equipped with a heating stage. The infrared and far infrared spectra were recorded by Messrs. S. Ishikawa and T. Yamamoto of Osaka University, to whom thanks are due. The authors acknowledge the referee for his useful suggestions, especially the alternate interpretation concerning the split C=O band.

References

1. G. W. Smith, *Advances in Liquid Crystals* (ed. by G. H. Brown, Academic Press, New York, 1975), Vol. 1, pp. 189–266.
2. G. W. Smith, *Comments Solid State Phys.*, **9**, 21 (1978).
3. A. R. Ubbelohde, *The Molten State of Matter* (John Wiley & Sons, New York, 1978).
4. S. Chandrasekhar, B. K. Sadashiva, and K. A. Suresh, *Pramāna* **9**, 471 (1977).
5. J. Billard, J. C. Dubois, T. N. Huu, and A. Zann, *Nouv. J. Chim.*, **2**, 535 (1978).
6. T. N. Huu, J. C. Dubois, J. Malthete, and C. Destrade, *C.R. Acad. Sci. (Paris)*, **286**, C463 (1978).
7. J. C. Dubois, *Ann. Phys.*, **3**, 131 (1978).
8. A. Bêguin, J. Billard, J. C. Dubois, T. N. Huu, and A. Zann, *J. de Phys.*, **40**, C3–15 (1979).
9. C. Destrade, M. C. Mondon, and J. Malthete, *J. de Phys.*, **40**, C3–17 (1979).
10. A. M. Levelut, *J. de Phys.*, **40**, L–81 (1979).
11. C. Destrade, M. C. Mondon-Bernaud, and T. N. Huu, *Mol. Cryst. Liq. Cryst. (Letters)*, **49**, 169 (1979).
12. S. Chandrasekhar, B. K. Sadashiva, K. A. Suresh, N. V. Madhusudana, S. Kumar, R. Shashidhar, and G. Venkatesh, *J. de Phys.*, **40**, C3–120 (1979).
13. F. A. Hoglan and E. Bartow, *J. Am. Chem. Soc.*, **62**, 2397 (1940).
14. I. E. Neifert and E. Bartow, *J. Am. Chem. Soc.*, **65**, 1770 (1943).
15. *Organic Syntheses*, Coll. Vol. 5, 595 and 1011 (1973).
16. M. Yoshikawa, K. Tsuji, M. Sorai, H. Suga, and S. Seki, to be published.
17. M. Sorai and S. Seki, *J. Phys. Soc. Japan*, **32**, 382 (1972).
18. R. H. Beaumont, H. Chihara, and J. A. Morrison, *Proc. Phys. Soc.*, **78**, 1462 (1961).
19. S. Blasenbrey and W. Pechhold, *Rheologica Acta*, **6**, 174 (1967).
20. T. H. Goodwin, M. Przybylska, and J. M. Robertson, *Acta. Cryst.*, **3**, 279 (1950).
21. G. D. Oliver, M. Eaton, and H. M. Huffman, *J. Am. Chem. Soc.*, **70**, 1502 (1948).
22. J. F. Messerly and H. L. Finke, *J. Chem. Thermodyn.*, **2**, 867 (1970).

23. H. M. Huffman, G. S. Parks, and A. C. Daniels, *J. Am. Chem. Soc.*, **52**, 1547 (1930).
24. M. E. Spaght, S. B. Thomas, and G. S. Parks, *J. Phys. Chem.*, **36**, 882 (1932).
25. M. Momotani, H. Suga, S. Seki, and I. Nitta, *Proc. Natl. Acad. Sci. (India)*, **25**, A74 (1956).
26. M. Frankosky and J. G. Aston, *J. Phys. Chem.*, **69**, 3126 (1965).
27. J. G. Aston and G. H. Messerly, *J. Am. Chem. Soc.*, **62**, 1917 (1940).
28. G. H. Messerly and R. M. Kennedy, *J. Am. Chem. Soc.*, **62**, 2988 (1940).
29. D. R. Douslin and H. M. Huffman, *J. Am. Chem. Soc.*, **68**, 1704 (1946).
30. H. L. Finke, M. E. Gross, G. Waddington, and H. M. Huffman, *J. Am. Chem. Soc.*, **76**, 333 (1954).
31. A. A. Schaerer, C. J. Busso, A. E. Smith, and L. B. Skinner, *J. Am. Chem. Soc.*, **77**, 2017 (1955).
32. J. D. Hoffman, *J. Chem. Phys.*, **20**, 541 (1952).
33. G. B. Guthrie and J. P. McCullough, *J. Phys. Chem. Solids*, **18**, 53 (1961).
34. R. H. Aranow, L. Witten, and D. H. Andrews, *J, Phys. Chem.*, **62**, 812 (1958).
35. T. G. Coker, J. Ambrose, and G. J. Janz, *J. Am. Chem. Soc.*, **92**, 5293 (1970).
36. T. G. Coker, B. Wunderlich, and G. J. Janz, *Trans. Faraday Soc.*, **65**, 3361 (1969).
37. A. Bondi, *Chem. Rev.*, **67**, 565 (1967).
38. J. Timmermans, *J. Chim. Phys.*, **35**, 331 (1938).
39. M. Postel and J. G. Riess, *J. Phys. Chem.*, **81**, 2634 (1977).